

Effect of thermal treatment on the surface morphology and wettability of hydroxyapatite films deposited by rf magnetron sputtering

A.C. PARAU^{a,b}, A.E. KISS^a, V. BRAIC^a, M. BALACEANU^a, I. PANA^a, A. VLADESCU^{a*}

^a*Institute for Optoelectronics, 409 Atomistilor, 077125, Magurele-Bucharest, Romania*

^b*University of Politehnica of Bucharest, 313 Spl. Independentei, 060042, Bucharest, Romania*

The hydroxyapatite (HAP) ceramic, widely used as a biological active coating for the metallic implants in arthroplasty, presents different characteristics depending on the synthesis process. The surface characteristics such as its surface chemistry, surface energy, topography and roughness are important properties to be determined when considering the use of an implant. In the present work, the magnetron sputtering deposition method was used to deposit HAP coatings on Ti6Al4V alloy, in order to investigate the effect of thermal treatment on their surface roughness and wettability. The coatings were investigated for their composition and crystallographic structure by EDX, FT-IR and XRD, as well for their surface morphology by SEM and stylus based surface profilometry. The assessment of the wettability was done by using the sessile drop method, the contact angles for various liquids, the surface free energy and the work of adhesion on water being determined. After annealing the HAP coatings became crystalline, preserved their elemental composition, but exhibited different surface roughness and work of adhesion on water.

(Received September 17, 2012; accepted October 30, 2012)

Keywords: Hydroxyapatite coatings, Magnetron sputtering, Roughness, Contact angle

1. Introduction

The hydroxyapatite (HAP) ceramic is a widely used biological active coating for the metallic implants used in arthroplasty. It is composed of the essential elements of human tissues, as calcium and phosphorus ($\text{Ca}_5(\text{PO}_4)_3\text{OH}$), being chemically similar to the main inorganic constituent of natural bone, which is a carbonate-containing calcium deficient hydroxyapatite [1]. Due to its composition and porous structure, the synthetic HAP coating is inherent biocompatible, forming a strong bond with the bone [2].

However, HAP coatings present different characteristics depending on the synthesis process. It is known that the crystalline HAP is a better alternative to the amorphous one, as it is less prone to dissolve in the biological surrounding fluids [3, 4]. The surface characteristics of HAP coatings, as the surface chemistry, surface energy and topography, are important properties to be considered for implant coating [5–7].

In the present work, the magnetron sputtering deposition method is used to prepare HAP coatings on a Ti6Al4V alloy, in order to investigate the effect of thermal treatment (performed under different conditions) on the surface roughness and wettability of hydroxyapatite films.

2. Experimental details

2.1. Materials

The Ti6Al4V alloy was cut into discs with 20 mm diameter. A HAP disc, 1" diameter, 99.9% purity, from Kurt J. Lesker Company, was used as magnetron target for depositing thin films. The target and substrate materials were ultrasonically cleaned with acetone, ethanol and de-ionized water for 10 min.

2.2. Magnetron deposition

The base pressure in the deposition chamber was 1.3×10^{-4} Pa. The deposition was done in Ar atmosphere at 6.6×10^{-1} Pa. The main deposition parameters were as follows: RF power fed on cathode: 50 W; substrate bias voltage: -60 V; substrate temperature: 80^o C; distance cathode-substrates: 25 mm. The thickness of the HAP coatings was of about 350 nm.

2.3. Thermal annealing

After deposition, the samples were annealed in a computer controlled oven, for 30 and 120 minutes at 600°C and 800°C, with an annealing gradient of 12°C/min, in a flux of dry nitrogen and water vapours.

2.4. Elemental and phase composition

Energy dispersive X-ray analysis (EDX) was used to investigate the elemental composition of the coatings. EDX analysis was carried out on a scanning electron microscope (XL-30 – ESEM TMP), equipped with energy dispersive X-ray spectroscopy. An average composition was obtained by measuring in 3 different points on the material surface.

Fourier transform infrared spectroscopy (FTIR) of the samples were carried out using a Jasco FT/IR 6300 spectrometer, 4 cm⁻¹ resolution and 16 scans using an ATR (Attenuated Total Reflectance) unit, which permits the spectra collection without any special sample preparation. The range of frequencies was from 350 to 4000 cm⁻¹. In order to obtain a good signal-to-noise ratio, ten scans were collected and averaged.

The phase compositions of the HAP target, Ti6Al4V alloy and of the films were determined by X-ray diffraction analysis (Rigaku MiniFlex II, with Cu K α radiation).

2.5 Surface morphology

Surface roughness parameters were measured with a Dektak 150 surface profiler with a low-inertia stylus sensor (12.5 mm radius). The measurement was taken on 4 mm scan length with 48 μ N contact force and 20 μ m/s scan speed. Ten profilometry measurements were made for each specimen and a mean value was calculated. There were determined the following roughness parameters: R_a - average roughness, R_q - root-mean-square roughness, and S_{skw} - skewness, representing the symmetry of the profile about the mean line. They were obtained from the following equations:

$$R_a = \frac{1}{n} \sum_{i=1}^n |y_i| \quad (1)$$

$$R_q = \sqrt{\frac{1}{n} \sum_{i=1}^n y_i^2} \quad (2)$$

$$S_{skw} = \frac{1}{nR_q^3} \sum_{i=1}^n y_i^3 \quad (3)$$

The surface morphology was also observed by scanning electron microscopy, using a XL-30 – ESEM TMP microscope.

2.6. Contact-angle measurement

The wetting properties of the Ti6Al4V alloy, of the as deposited HAP and thermal annealed HAP surfaces were studied by measuring the contact angle between the surface and different liquids droplets, using a standard Hamilton micro-syringe (1 ml). The test was conducted in air at 20 °C, using an Attension TL101 tensiometer (KSV-

Instruments). The mean value for the angle was the average of five measurements for each sample, deposited on different regions.

The coatings' surface free energy (γ_s^{tot}) was calculated by measuring the contact angle between the samples and the drops of three different liquids with known surface tension polar (γ_L^p) and dispersive (γ_L^d) components [8]. The liquids were chosen to cover the largest possible range from highly polar (water) to almost completely non-polar liquid (diiodomethane).

In Table 1, the values of components of the surface free energy of the liquids used in the determinations are given.

Table 1. The surface tension parameters of the liquids used for surface free energy determination.

Liquid	γ_L^{tot} (mJ/m ²)	γ_L^d (mJ/m ²)	γ_L^p (mJ/m ²)
deionised water	72.8	21.8	51
ethylene glycol	48.0	29.0	19
diiodomethane	50.8	50.8	0

3. Results and discussions

3.1. Elemental and phase composition

EDX analysis of the coatings reveals that all the Ca/P ratios are close to 1.67, which corresponds to a stoichiometric HAP, as presented in Table 2. The data were calculated by excluding the signal from the Ti6Al4V substrate. The oxygen concentration, higher than expected, is probably due to the signal arising from the native titanium oxide formed on the Ti6Al4V surface, adsorbed oxygen due to the porosity of the coating, and the overestimation of the oxygen in EDX analysis. As an example, Fig. 1 shows the EDX spectrum performed on the HAP sample annealed at 600°C for 120 min. As the HAP coatings are relatively thin, the spectrum also contains the signature of the substrate elements (Ti, Al and V), as well as some oxygen from the native oxide formed at the alloy surface.

Table 2. The EDX composition of the HAP coatings

Coating	Annealing conditions		Elemental composition (at. %)			
	Temp (°C)	Duration (min)	O	Ca	P	Ca/P
HAP - 1	-	-	83.1	10.5	6.4	1.63
HAP - 2	600	30	93.6	4.0	2.4	1.63
HAP - 3	600	120	94.0	3.7	2.2	1.66
HAP - 4	800	30	93.8	3.8	2.3	1.65
HAP - 5	800	120	94.2	3.5	2.1	1.67

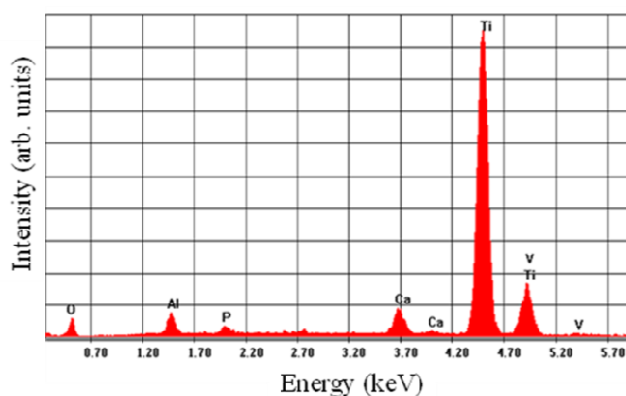


Fig. 1. The EDX spectrum of the HAP coating annealed at 6000C for 120 min.

FTIR analysis (Fig.2) gives the infrared spectrum of absorption bands, so it was possible to find some bands attributable to HAP, in both as-deposited and annealed films. Some of the HAP absorption bands were identified, as presented in the following. In HAP-1 coating, the bands were attributed to HAP - ν_4 (571 cm^{-1}) and ν_3 (1083 cm^{-1}) bands, to CO_3^{2-} - ν_3 mode (1640 cm^{-1}) and to hydroxyl band (3570 cm^{-1}). In HAP-2 sample, the bands were identified as HAP - ν_1 (962 cm^{-1}), ν_2 (462 cm^{-1}), and ν_4 (571 cm^{-1}) bands, as well as the CO_3^{2-} - ν_3 mode (1640 cm^{-1}) and the hydroxyl band (3570 cm^{-1}). In HAP-3, only the HAP - ν_4 (601 cm^{-1}) band and a weak hydroxyl band (3570 cm^{-1}) were observed. In FTIR spectra of HAP-4, two HAP bands are present: ν_1 at 962 cm^{-1} , and ν_4 at 571 cm^{-1} , while for HAP-5 only the HAP - ν_4 band at 571 cm^{-1} is still visible. It is to note that the hydroxyl signature vanished from the FTIR spectra after the annealing process, even if it was done in water vapours. Also, the signature associated with a stoichiometric HAP around 1100 cm^{-1} was observed in all HAP coatings.

The XRD pattern of the Ti6Al4V substrates and of the HAP target are presented in Fig. 3, along with the patterns obtained for the HAP coatings. The as-deposited HAP films were amorphous, as reported by almost all groups working with magnetron sputtering method [9, 10–13]. The films crystallized after the thermal annealing process. The position of the main peaks corresponding to HAP target are indicated by dashed red lines, while the ones corresponding to the substrate by dotted black lines. All the annealed coatings could be identified as crystalline HAP (JCPDS 9-432/2000). In our case, no extra phases, which could be ascribed to other systems, could be detected from the XRD patterns. If present, the extra phases such as calcium oxide (JCPDS 37-1497/2000) or β -tricalcium phosphate (JCPDS 9-169/2000) should have a Ca/P ratio much higher or much lower than 1.6, the value actually resulted from EDX analysis.

Previously reported investigations [14, 15] have demonstrated the role of water vapour during annealing, in the process of HAP crystallization. It seems that the presence of moisture in the annealing process promotes the crystallization of HAP [14, 15]. As seen in the XRD

diffraction patterns, the patterns of the annealed HAP coatings and HAP target are quite similar, especially if the same values would be used on the ordinate OY scale (not shown here, due to the large signal arising from the alloy substrate). A higher annealing temperature was found to favour the film crystallization, as observed from the increased intensity of the (201) and (302) peaks for the samples annealed at 800°C , which agrees with other reported results [14, 16].

3.2. Surface roughness and morphology

The average surface roughness (R_a) gives an overall description of height variations, but does not give any information on the wavelength and it is not sensitive to small changes in the surface profile. However, the root mean square roughness (R_q) is more sensitive to deviations from the main line than R_a . According to the ISO 4287 standard, the skewness S_{skw} is sensitive on occasional deep valleys or high peaks.

The roughness parameters R_a , R_q and S_{skw} of the coatings are summarized in Table 3. For comparison, it was also presented the roughness parameters of the uncoated substrate. One may observe that the roughness parameters R_a and R_q increased as compared to the substrate, and further after annealing, in a direct relation with the annealing temperature and treatment duration.

One may also observe that the skew negative values of coatings are higher (in modulus) than that of the substrate and the modulus value increases with the annealing temperature and duration. The negative values of the skewness indicate a predominance of valleys and the lack of protruding peaks above a flattered average. As the skewness represents a probability distribution, an increasing skewness value implies that the shapes of the individual valleys are more diverse, which is to be expected for the HAP coatings which have undergone a thermal annealing at a higher temperature and for a longer period. As reported in the literature [17], an increased roughness of the contact surface and more negative values of the S_{skw} parameter often present an advantage in terms of friction, as the use of surfaces with more negative skewness always determines lower friction coefficients.

The surface morphology of HAP coatings, observed by SEM, is presented in Fig. 4, which reveals the increase of the roughness with the annealing duration and temperature, without the presence of micron-sized particles, as observed in pulsed laser deposited HAP coatings [18, 19].

From SEM images, one can observe that the surface of the HAP-2 coating is covered with some white spots, which represents local region with oxidation products, most probably phosphorous oxides, as reported in the literature [20].

3.3. Contact-angle results

The measured contact angle values of the samples, in deionised water, ethylene glycol, glycerol and diiodomethane, are presented in Table 4. The displayed

values are the results of 5 different measurements, the standard deviation being also calculated.

The contact angle θ_C is a macroscopic quantity, and it is useful in the characterization of the wetting properties of a surface, even though the latter is actually determined by the microscopic properties of the material. Young [21] observed more than two hundred years ago that the contact angle, θ_C , is related to the surface tensions pertaining to the relevant interfaces, γ_{ij} , where ij can be sv (solid-vapor), sl (solid-liquid), and lv (liquid-vapor) in the following way:

$$\cos \theta_C = \frac{\gamma_{sv} - \gamma_{sl}}{\gamma_{lv}} \quad (4)$$

known as the Young-Dupré relation [22].

The surface free energy of a solid surface gives a direct measurement of intermolecular interactions at interfaces, having a strong influence on wetting, adsorption and adhesion behaviour [23].

Considering the contact of one liquid (L) on one solid surface (S), in an environment equivalent to air, the work of adhesion of the liquid on the solid surface can be expressed as:

$$W_{adh} = \gamma_S + \gamma_L - \gamma_{SL} \quad (5)$$

where γ_L and γ_{LS} are the surface energies of the liquid and solid, respectively, and γ_{SL} is the surface energy of the liquid on the solid surface.

Since the adhesion is due to London dispersion forces, γ^d , and to polar forces such as hydrogen bonding γ^p , Fowkes [24] has described the γ_{SL} as:

$$\gamma_{SL} = \gamma_S + \gamma_L - 2\sqrt{\gamma_S^p \gamma_L^p} - 2\sqrt{\gamma_S^d \gamma_L^d} \quad (6)$$

By introduction of the equation (6) in the eq. 5, the expression for work adhesion of the liquid to the solid surface in air is:

$$W_{adh} = 2\sqrt{\gamma_S^p \gamma_L^p} + 2\sqrt{\gamma_S^d \gamma_L^d} \quad (7)$$

As the surface tension parameters of the used liquids are known from the literature (Table 1), we used the Fowkes approach to determine the total surface free energy γ_s^{tot} of the samples, comprising the dispersive γ_s^d and the polar γ_s^p parts, as presented in Table 4.

The contact angle between a solid and a liquid represents the mixed result of the chemical (chemical bonding), physical (physical bonds, as promoted by the van der Waals and other non-covalent interactions) and mechanical (mainly surface roughness) interactions between the two media [25]. So, a high contact angle is the result of a small surface area between the liquid and solid, determining a low surface energy and a high work of adhesion.

Our results show the decrease of the work of adhesion of all HAP coatings, as compared with the substrate alloy. The contact angle between liquid and HAP coating is a function of dispersive adhesion (due to the interaction between the liquid and solid molecules), and of the cohesion (due to the interaction between the liquid molecules themselves). In the studied cases, a low adhesion and a strong cohesion resulted in a relatively poor wetting, as relatively high contact angles were measured, except for the HAP-3 coating. The last result demonstrates that the crystalline HAP coating obtained after annealing at 600°C for two hours, due to its high wettability, represents a good candidate as ceramic biocompatible coating to be used for medical implants.

Table 3. Roughness parameters of the investigated samples

Sample	R _a (μm)	R _q (μm)	S _{skw}
Ti6Al4V	0.054±0.002	0.070±0.003	-0.01±0.10
HAP - 1	0.292±0.096	0.369±0.108	-0.15±0.08
HAP - 2	0.330±0.161	0.422±0.175	-0.39±0.07
HAP - 3	0.378±0.071	0.463±0.072	-0.65±0.04
HAP - 4	1.152±0.139	1.339±0.283	-0.83±0.01
HAP - 5	1.416±0.203	1.672±0.253	-0.81±0.01

Table 4. Contact angles, the total surface free energy, its polar and dispersed components, and the work of adhesion for water, of the investigated surfaces

Sample	Contact angle θ ($^{\circ}$)			Surface tension parameters			W_{adh}^{water} (mN/m)
	water	ethylene	di-iodomethane	γ_s^{tot} (mN/m)	γ_s^d (mN/m)	γ_s^p (mN/m)	
Ti6Al4V	67.09±2.07	43.65±1.21	48.10±0.84	43.27	33.29	9.98	99.00
HAP - 1	70.32±0.03	84.22±1.49	55.81±2.15	31.43	24.86	6.57	83.16
HAP - 2	83.04±0.95	40.79±0.02	32.99±0.18	45.33	43.22	2.11	82.14
HAP - 3	54.73±0.02	94.91±1.30	40.98±0.25	36.57	27.98	8.58	91.25
HAP - 4	101.56±7.97	98.92±4.39	56.26±1.04	28.04	27.71	0.32	57.28
HAP - 5	108.81±7.04	78.69±5.16	53.22±3.13	32.10	32.03	0.08	56.81

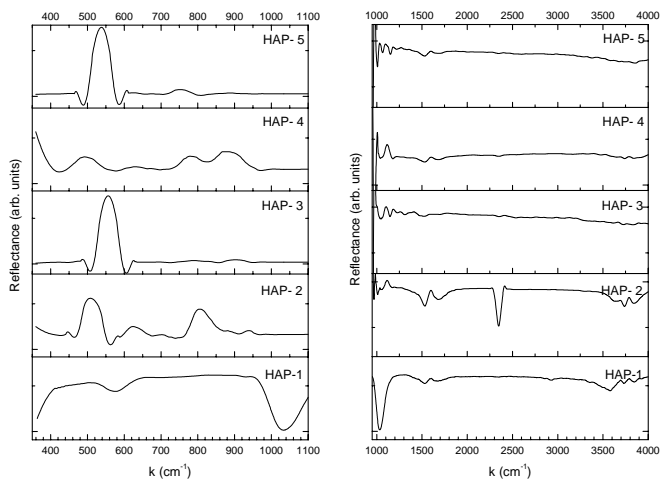


Fig. 2. The FT-IR spectra of the HAP coatings

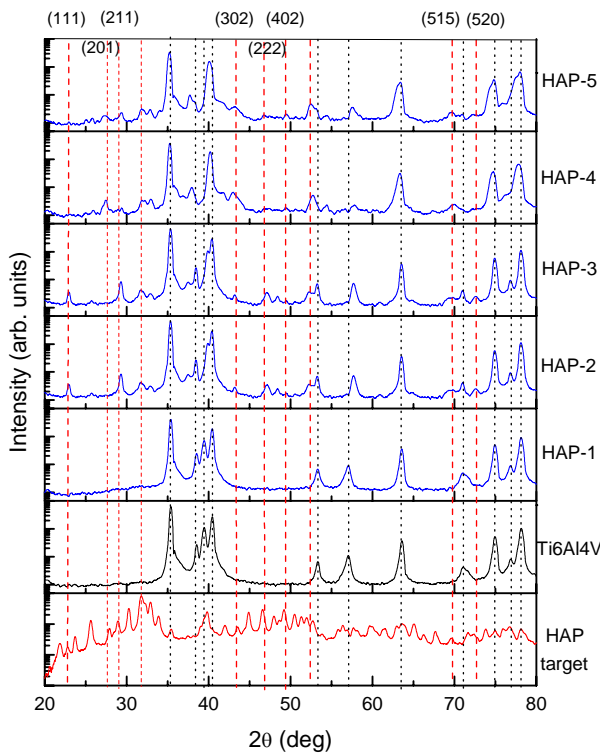


Fig. 3. XRD patterns of the HAP target, substrate Ti6Al4V alloy, and HAP deposited films.

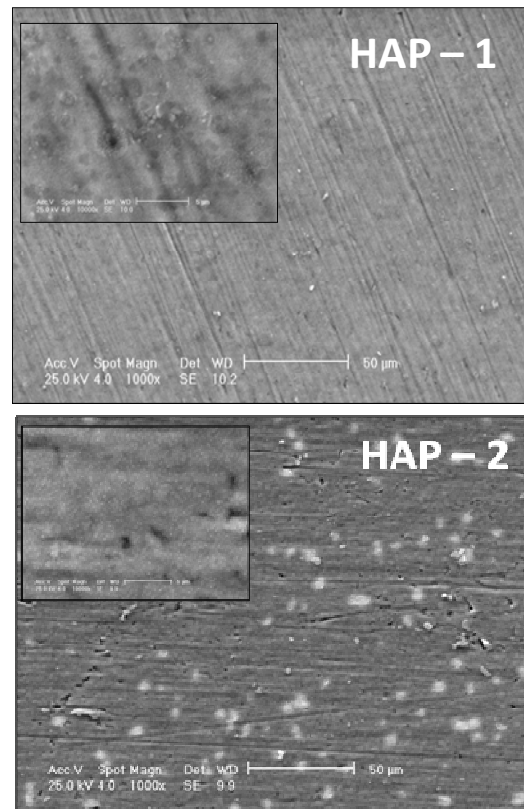


Fig. 4. SEM images of the as-deposited HAP coating (HAP-1, with an insert for a higher resolution) and annealed at 600°C for 30 min (HAP-2)

4. Conclusions

In the present work, the RF magnetron sputtering deposition method is used to form HAP coatings, with a thickness of about 350 nm, on Ti6Al4V alloy substrates. The as-deposited HAP coatings were amorphous. To promote their crystallization, the samples were annealed in an oven for 30 and 120 minutes at 600 °C and 800 °C, in a flux of dry nitrogen and water vapours.

The elemental analysis revealed that all the coatings presented Ca/P ratios close to 1.67, indicating the formation of a stoichiometric HAP.

By FTIR analysis, some bands attributable to HAP were evidenced, in both as-deposited and annealed films.

The signature associated with a stoichiometric HAP around 1100 cm^{-1} was observed in all coatings.

All the annealed coatings could be identified as crystalline HAP, no extra phases being detected.

The roughness parameters R_a and R_q increased as compared to the substrate, and further after annealing, in a direct relation with the annealing temperature. The modulus of the negative skew of all the coatings are higher than that of the substrate, and the modulus values increase, as expected, with the annealing temperature and period, implying that the shapes of the individual valleys are increasingly divers.

The obtained results show a lower work of adhesion of all HAP coatings, as compared with the substrate.

We have demonstrated that the crystalline HAP coating obtained after annealing the as-deposited HAP at $600\text{ }^\circ\text{C}$ for two hours, due to its high wettability, represents a good candidate as ceramic biocompatible coating to be used for medical implants.

Acknowledgement

This work was supported by a grant of the Romanian National Authority for Scientific Research, CNCS - UEFISCDI the project number PN-II-RU-TE-2011-3-0284 (90%), and by the Sectoral Operational for Human Resources Programme POSDRU- 88/1.5/S/60203 (10%).

References

- [1] J.C. Elliot, Structure and Chemistry of the Apatites and Others Orthophosphates, Elsevier, Amsterdam, 1994.
- [2] K.A. Hing, S.M. Best, W. Bonfield, J. Mater. Sci. Mater. Med., **10**, 135 (1999).
- [3] K. Ozeki, T. Yuhta, Y. Fukui, H. Aoki, Surf. Coat. Technol. **160**, 54 (2002).
- [4] R.Z. LeGeros, Clin. Mater., **14**, 65 (1993).
- [5] R.Z. LeGeros, R.G. Craig, J. Bone Miner. Res. **8**, S583 (1993).
- [6] J.M. Lee, J.I. Lee, Y.J. Lim, Appl. Surf. Sci., **256**, 3086 (2010).
- [7] B.-D. Hahn, D.-S. Park, J.-J. Choi, J. Ryu, W.-H. Yoon, J.-H. Choi, J.-W. Kim, Y.-L. Cho, C. Park, H.-E. Kim, S.-G. Kim, Appl. Surf. Sci. **257**, 7792 (2011).
- [8] F. Pinzari, P. Ascarelli, E. Cappelli, G. Mattei, R. Giorgi, Diamond Relat. Mater., **10**, 781 (2001).
- [9] K. van Dijk, H.G. Schaeken, J.G.C. Wolke, J.A. Jansen, Biomaterials, **17**, 405 (1996).
- [10] J.L. Ong, L.C. Lucas, Biomaterials, **15**, 337 (1994).
- [11] Y. Yang, K. Kim, C.M. Agrawal, J.L. Ong, Biomaterials, **24**, 5131 (2003).
- [12] E.S. Thian, J. Huang, S.M. Best, Z.H. Barber, W. Bonfield, Biomaterials, **26**, 2947 (2005).
- [13] J.G.C. Wolke, K. de Groot, J.A. Jansen, J. Biomed. Mater. Res., **39**, 5247 (1998).
- [14] J.M. Fernandez-Pradas, L. Clèries, E. Martinez, G. Sardin, J. Esteve, J.L. Morenza, Appl. Phys., **A 71**, 37 (2000).
- [15] J. Weng, Y. Cao, J.Y. Chen, X.D. Zhang, J. Mater. Sci. Lett., **14**, 211 (1995).
- [16] H.T. Zeng, W.R. Lacefield, S. Mirov, J. Biomed. Mater. Res., **50**, 248 (2000).
- [17] M. Sedlaček, L. M. Silva Vilhena, B. Podgornik, J. Vižintin, J. Mechan. Eng., **57**, 674 (2011).
- [18] F. Sima, C. Ristoscu, N. Stefan, G. Dorcioman, I.N. Mihailescu, L.E. Sima, S.M. Petrescu, E. Palcevskis, J. Krastins, I. Zalite, Appl. Surf. Sci., **255**, 5312 (2009).
- [19] H.C. Man, K.Y. Chiu, F.T. Cheng, K.H. Wong, Thin Solid Films, **517**, 5496 (2009).
- [20] E. Zhang, C. Zou, Acta Biomater, **5**, 1732 (2009).
- [21] T. Young, An essay on the cohesion of fluids, Philos. Trans. R. Soc. London, **95**, 65 (1805).
- [22] D. Quere, Physica, A **313**, 32 (2002).
- [23] E.R. Ionita, M.D. Ionita, E.C. Stancu, M. Teodorescu, G. Dinescu, Appl. Surf. Sci., **255**, 5448 (2009).
- [24] F.W. Fowkes, J. Phys. Chem., **67**, 2538 (1963).
- [25] A. W. Adamson, A. P. Gast, Physical Chemistry of Surfaces, Wiley Interscience, New York, 1997.

*Corresponding author: alinava@inoe.ro